Available online at www.sciencedirect.com
ScienceDirect
Trans. Nonferrous Met. Soc. China 33(2023) 1655−1664
Transactions of Nonferrous Metals Society of China
www.tnmsc.cn

In-situ evidence for rotation of Si particles with respect to grains in tensile-deformed Al−Si alloys

Yao XIAO[1], Xin-yue LAN[1], Qiang LU[1], Yong DU[1,2,3], Kai LI[1,2,3]

1. State Key Laboratory of Powder Metallurgy, Central South University, Changsha 410083, China;
2. National Key Laboratory of Science and Technology for National Defense on High-strength Structural Materials, Central South University, Changsha 410083, China;
3. Advanced Research Center, Central South University, Changsha 410083, China

Received 26 January 2022; accepted 5 April 2022

Abstract: To clarify whether the Si particles rotate with respect to the matrix grains during tensile deformation of Al−Si alloys, in-situ tensile SEM and ex-situ EBSD were coupled to investigate the relationship between Si particles' rotation and grain rotation. By comparing the on-plane projection of 3D orientations of grains revealed by EBSD and in-situ SEM observations of Si particles during deformation, noticeable relative rotation of Si particles on the sample surface plane with respect to the matrix grains was found. Besides, greater relative rotation of the Si particle was found to introduce a higher density of geometrically necessary dislocations (GNDs) which can cause work-hardening effects in the matrix nearby the Si particles, according to kernel average misorientation (KAM) analysis of EBSD data. In summary, the larger relative rotation of Si particles can cause higher work-hardening effects.

Key words: Al−Si alloy; relative rotation; geometrically necessary dislocation; in-situ tension; plastic deformation; work-hardening effect

1 Introduction

In hard particle reinforced composites with soft matrix, the applied external force affects the rotation of the hard particles [1] and this rotation is considered to have very important influence on the mechanical properties [2]. Al−Si alloys with reinforcing Si particles and soft α(Al) matrix, are systems of this kind. They have high specific strength and good castability, and are thus widely used in the automotive and aerospace fields [3−5]. Strengthening and toughening of Al−Si alloys are becoming more and more important with the development of these industries. Understanding the Si particles' rotation under external force in the alloys is the prerequisite of adjusting the micro-structure and increasing the overall mechanical properties.

The grain rotation has been intensively investigated in the current research of the deformation mechanism of metallic materials. For example, many researchers [6−8] found that during the plastic deformation process, the grains from the nano- to micro-scales in different types of alloys rotated to prevent local severe stress concentration. NAGARAJAN et al [9] pointed out that if the lattice rotation (of a grain) along one direction was interrupted locally by a rigid second phase, it could introduce additional rotation along other directions.

In studies concerning deformation behaviors of second-phase particles in alloys, the main focus is on how the second-phase particles affect grain rotation, and how the particles rotate during the deformation with respect to the deformation directions. For example, AGRAWAL et al [10] used

Corresponding author: Kai LI, Tel: +86-18973163497, E-mail: leking@csu.edu.cn
DOI: 10.1016/S1003-6326(23)66211-9

stereological methods to statistically analyze the rotation behaviors of micro-scale Fe-containing particles in extruded 6061 aluminum alloys and found that the tensile deformation along the extrusion direction hardly caused rotation of the particles; however, obvious rotation of particles was found in torsion and compression. FONSECA and KO [11] used the HRDIC (high-resolution digital image correlation) method to study the influence of Si particles on the plastic deformation of the matrix in an Al−Si alloy. It was found that Si particles can cause the matrix's slip bands to intensify, broaden, bend and increase in number, which led to uneven deformation.

In this condition, it is important to study the relationship between the rotation of Si particles and that of the matrix grains for understanding the deformation mechanism of Al−Si alloys. In our recent work of an Al−Si alloy in as-cast or heat-treated states, it was found that particles with a characteristic angle of 0°−50° or 130°−180° (the angle between the long axis of the particles and the loading axis) are more likely to break [12]. However, whether the Si particles rotate relatively with respect to the grain nearby or in full accordance with grains, has not been experimentally investigated yet. The major technical difficulty is that the EBSD signal of micro-scale Si particles is too weak and their 3D orientation cannot be measured. Therefore, a systematic approach by comparing the 2D rotation of Si particles observed by in-situ SEM and the 3D orientations of matrix grains obtained by ex-situ EBSD, on the same sample surface plane, has been established in this work to clarify this question.

2 Experimental

2.1 Materials and methods

The raw materials, including pure Al (99.7%), pure Mg (99.99%), as well as Al−20%Si, Al−10%Mn, Al−10%Fe, Al−10%Sr, and Al−5%Ti−1%B (all in wt.% unless specified) master alloys, were melted and cast in a vacuum-assisted die-casting instrument. The composition determined by inductively coupled plasma-atomic emission spectrometry (ICP-AES) is shown in Table 1. The addition of Sr and Ti+B is for refining Si particles and α(Al) matrix grains, respectively.

Table 1 Chemical composition of alloy (wt.%)

Si	Mg	Fe	Mn
7.2−8.1	0.22−0.32	0.11−0.25	0.19−0.26
Sr	Ti	B	Al
0.011−0.024	0.05−0.14	0.013−0.02	Bal.

In-situ tensile samples (as shown in Fig. 1) were taken from the castings, ground, polished, and ultrasonically cleaned. The in-situ tensile test was carried out on a Tescan Mira3 SEM equipped with a Mini-MTS@HT2000 in-situ tensile test machine (Qiyue Tech. Co., Ltd.). The load to the sample was paused and kept when the engineering strain was increased to 0.3%, 0.8%, 1.5%, 2.4%, 3.7%, 5.4%, 7.8%, 9.5% and 10.5%, respectively. The sample finally breaks at an engineering strain of 10.5%.

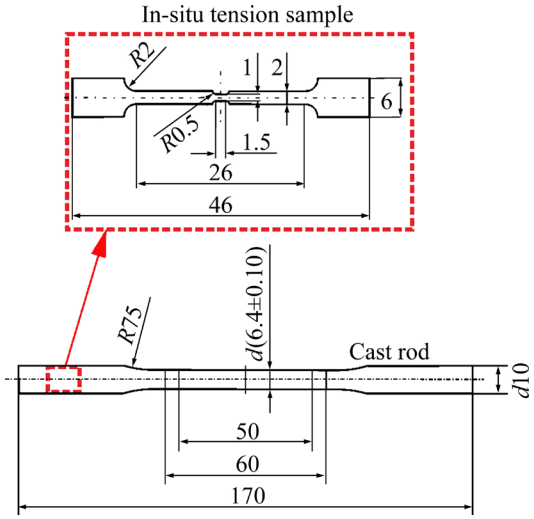

Fig. 1 Schematic diagram of preparation of in-situ tension sample from die-casting rod sample (unit: mm)

Both the cleaned sample and the tension-fractured sample were ex-situ observed by electron backscattering diffraction (EBSD) on a dual-beam scanning electron microscope (FEI Helios NanoLab G3 UC) to obtain the three-dimensional orientation of the α(Al) grains. EBSD measurements were conducted at an accelerating voltage of 30 kV and a beam current of 13 nA. The step size of EBSD scanning was 0.3 μm, which means that the spatial resolution can be expressed by the pixel size of 0.3 μm × 0.3 μm. The EBSD data were analyzed by Orientation Imaging Microscopy (OIM) Analysis software to obtain inversed pole figures (IPFs) and kernel average misorientation (KAM) images [13].

2.2 Processing of EBSD data

In this work, the relationship between particle rotation and grain rotation (in 3D) can only be compared on one plane (in 2D) due to the lack of EBSD signal of fine Si particles. Specifically, the particle rotation angle can only be measured under a 2D sample surface plane from secondary electron (SE) images, while the EBSD data include 3D information for the grain rotation. Therefore, the grain rotation projected on the sample surface plane, designated as the angle ω_g, needs to be calculated as follows.

Firstly, The Euler angles φ_1, ϕ and φ_2 can be obtained from each EBSD pattern. These data can be used to derive the following orientation matrix $\boldsymbol{G}$:

$$\boldsymbol{G}=\begin{pmatrix} \cos\varphi_1\cos\varphi_2-\sin\varphi_1\sin\varphi_2\cos\phi & \sin\varphi_1\cos\varphi_2+\cos\varphi_1\sin\varphi_2\cos\phi & \sin\varphi_2\sin\phi \\ -\cos\varphi_1\sin\varphi_2-\sin\varphi_1\cos\varphi_2\cos\phi & -\sin\varphi_1\sin\varphi_2+\cos\varphi_1\cos\varphi_2\cos\phi & \cos\varphi_2\sin\phi \\ \sin\varphi_1\sin\phi & -\cos\varphi_1\sin\phi & \cos\phi \end{pmatrix} \tag{1}$$

The rotation of a matrix grain during the tensile deformation is schematically shown in Figs. 2(a_1, a_2). The sample coordinate system, in which the rolling direction (RD), transverse direction (TD), and normal direction (ND) are defined as X, Y, and Z axes, respectively, is aligned such that the RD direction is parallel to the direction of tensile deformation in this work. The directions $[h_1, k_1, l_1]_g$ and $[h_2, k_2, l_2]_g$, expressed with the indices in the crystal coordinate system, are parallel to ND. Similarly, $[u_1, v_1, w_1]_g$ and $[u_2, v_2, w_2]_g$ are parallel to RD, and $[r_1, s_1, t_1]_g$ and $[r_2, s_2, t_2]_g$ are parallel to TD. The suffixes 1 and 2 denote the states before and after the grain rotation. In this work, these indices are normalized such that their moduli are equal to 1. Based on the experimentally determined $\boldsymbol{G}$ matrix by Eq. (1), the values of these indices can be obtained through the following equations:

$$\boldsymbol{G}_1=\begin{pmatrix} u_1 & r_1 & h_1 \\ v_1 & s_1 & k_1 \\ w_1 & t_1 & l_1 \end{pmatrix} \tag{2}$$

and

$$\boldsymbol{G}_2=\begin{pmatrix} u_2 & r_2 & h_2 \\ v_2 & s_2 & k_2 \\ w_2 & t_2 & l_2 \end{pmatrix} \tag{3}$$

According to these matrices, it is feasible to convert the indices in the crystal coordinate system into indices in the sample coordinate system and vice versa, the equations are shown as follows:

$$\boldsymbol{g}_g=\boldsymbol{G}\boldsymbol{g}_s \tag{4}$$

$$\boldsymbol{g}_s=\boldsymbol{G}^{-1}\boldsymbol{g}_g \tag{5}$$

where $\boldsymbol{g}_g$ is a direction expressed in the crystal

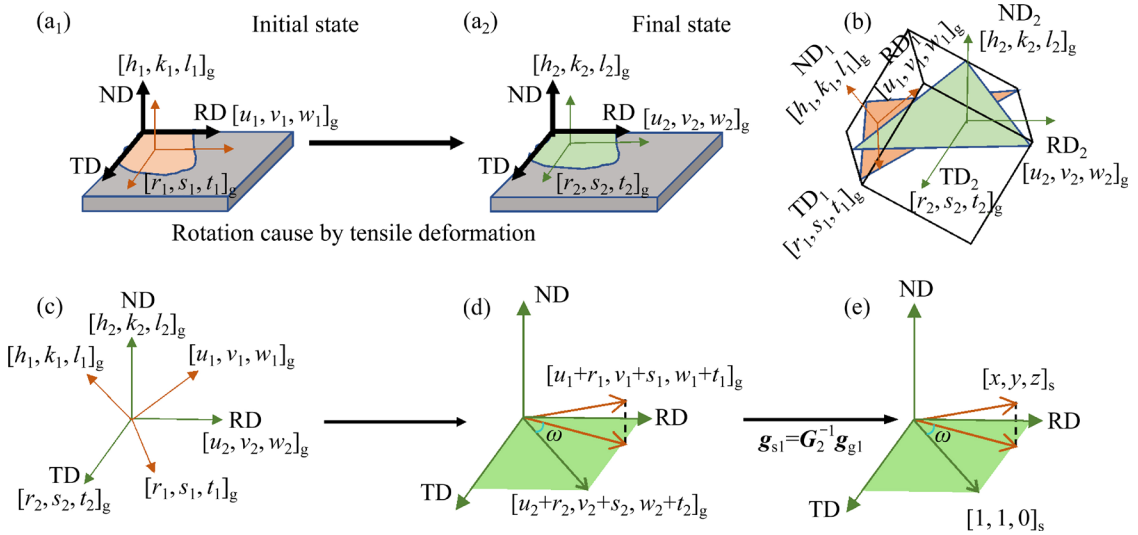

Fig. 2 Schematic of calculation of grain rotation (angle ω_g) projected on sample surface plane: (a_1, a_2) Initial and final orientations of grain during tensile deformation in sample coordinate system, respectively; (b) Rotation of grain from initial to final states in crystal coordinate system; (c) Vectors from (b) merged; (d) Two vectors selected for comparing on-plane grain rotation; (e) Two vectors expressed using sample coordinate system (transformed from $\boldsymbol{g}_g$ to $\boldsymbol{g}_s$) and angle

coordinate system and $\boldsymbol{g}_s$ in the sample coordinate system. $\boldsymbol{G}^{-1}$ is the inverse of the matrix $\boldsymbol{G}$ ($|\boldsymbol{G}|\neq 0$).

The orientations of the initial grain (RD_1, TD_1 and ND_1) and the rotated grain (RD_2, TD_2 and ND_2) with indices of the crystal coordinate system are shown in Fig. 2(b) and merged in Fig. 2(c). The $[h_1, k_1, l_1]_g$ direction is tilted during grain rotation to $[h_2, k_2, l_2]_g$ direction.

In the second step, the projection of the grain rotation on the RD−TD plane is best presented by the angle (i.e., ω_g) between the projection of the summed vectors $[u_1+r_1, v_1+s_1, w_1+t_1]_g$ and $[u_2+r_2, v_2+s_2, w_2+t_2]_g$, and they can be calculated as shown in Figs. 2(d) and (e). However, in a crystal coordinate system, it is hard to calculate the projection onto the sample surfaces plane, thus these vectors need to be transformed into the sample coordinate system (of the rotated state) by Eq. (5). By designating the sample coordinates as X, Y and Z, $[u_1+r_1, v_1+s_1, w_1+t_1]_g$ is transformed into $[x, y, z]_s$, and the $[u_2+r_2, v_2+s_2, w_2+t_2]_g$ direction is expressed as $[1, 1, 0]_s$, as shown in Fig. 2(e). The angle ω_g for the grain rotation projected on the sample surface plane, i.e., the angle between $[1, 1, 0]_s$ and $[x, y, 0]_s$, can now be calculated as

$$\omega_g = \arccos\left(\frac{[x,\ y,\ 0]_s \cdot [1,\ 1,\ 0]_s}{\sqrt{2}\ \|[x,\ y,\ 0]_s\|}\right) \tag{6}$$

It should be noted these calculations for the 3D-to-2D projection are based on the hypothesis that a rotation (of a particle) occurs with a relatively small rotation angle (e.g., <15°). Such a hypothesis holds true in Al alloys as no particle was observed with a rotation angle larger than 15° [14,15], and is consistent with the theoretical predictions according to the equations proposed in Ref. [1] based on complex potentials and conformal mapping methods.

3 Results and discussion

3.1 Relative rotation of Si particles

The engineering stress−strain curve recorded during the in-situ tensile experiment is shown in Fig. 3. Six states with strain ε=0, 2.4%, 5.4%, 7.8%, 9.5% and 10.5% were observed and shown in Fig. 4. During the tension process, the silicon particles progressively rotate relatively to the original state. The rotation of a typically elongated Si particle can be easily recognized unless the rotation axis is parallel (or nearly parallel) to its long axis.

The low magnification SEM images and IPFs at initial and final states are shown in Fig. 5. The elemental analysis from EDS spectra (Fig. 6) shows that the gray-contrast phase is Si particles, and the brighter phase is the α-$Al_{15}(Fe,Mn)_3Si_2$ phase [16−19]. The high magnification SEM images and the IPFs of the areas marked as rectangles in Fig. 5 are shown in Fig. 7.

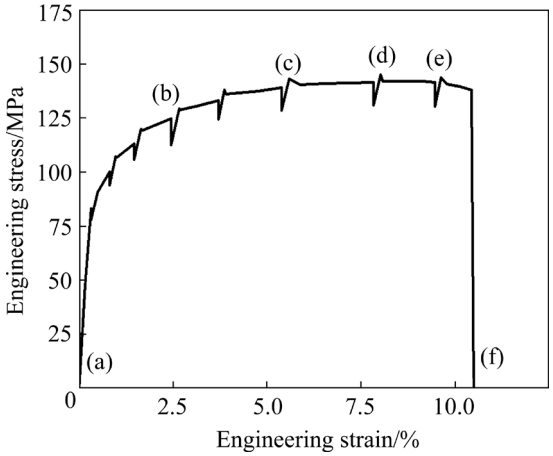

Fig. 3 Engineering stress−strain curve during in-situ tension

The signals from particles and grain boundaries were used as markers to accurately correlate the positions in second electron (SE, collected before a EBSD scan), EBSD and SE-II (collected during the same EBSD scan) images. The Si particles and the Al matrix both belong to the cubic crystal system and produce very similar Kikuchi lines [20], meanwhile the Si particles are very small (with diameters around 200 nm), thus the EBSD signals of Si particles are too low for a satisfactory resolution. After deformation, the surface roughness of the sample increases, hence the corresponding EBSD signals decrease abruptly in some areas [21,22] which appear dark as shown in Fig. 7(f). In the example of the region shown in Fig. 7, SE-II images in Figs. 7(b) and (e) are shown together with IPFs in Figs. 7(c) and (f), revealing the bright contrast from particles mostly located at grain boundaries. In comparison, more details of the particle morphology and cracks were obtained in the high-resolution SE images as shown in Figs. 7(a) and 7(d), due to the shorter scanning steps. By comparing these images, it is possible to correlate the positions (e.g., (1), (2), (3), and (4)) in these three types of images with satisfactory precision.

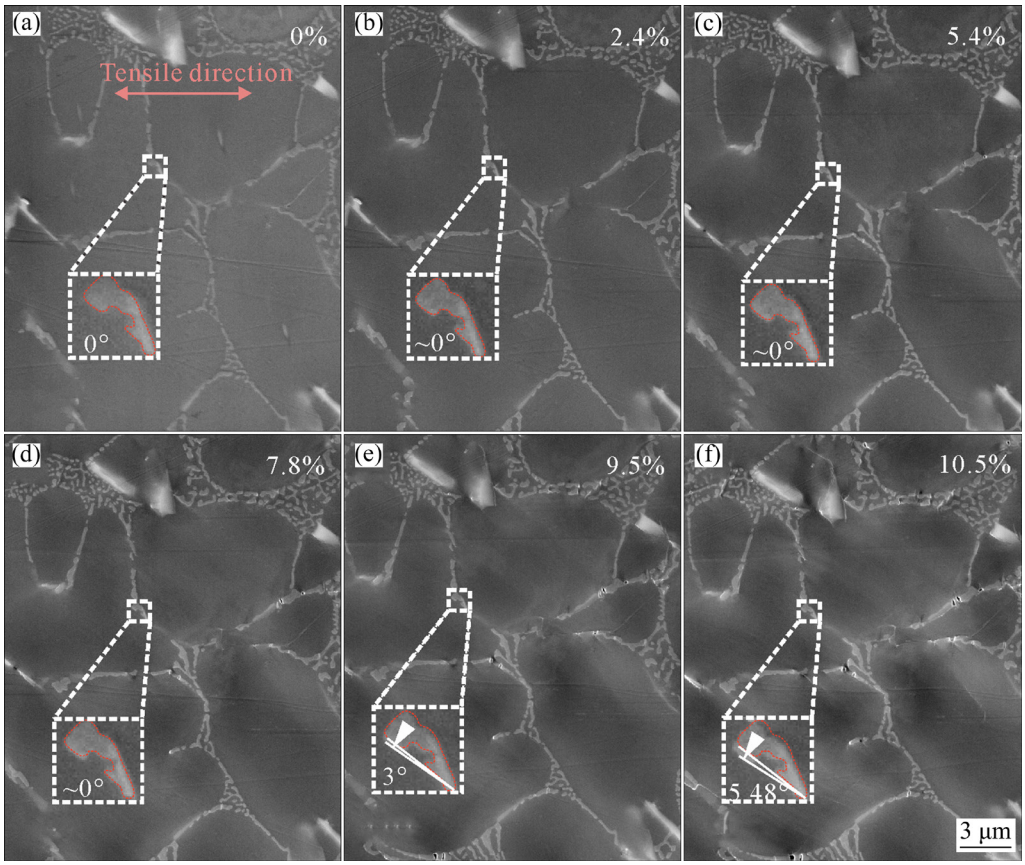

Fig. 4 SEM images of same area in Fig. 3 during in-situ tension at different strains: (a) 0%; (b) 2.4%; (c) 5.4%; (d) 7.8%; (e) 9.5%; (f) 10.3%

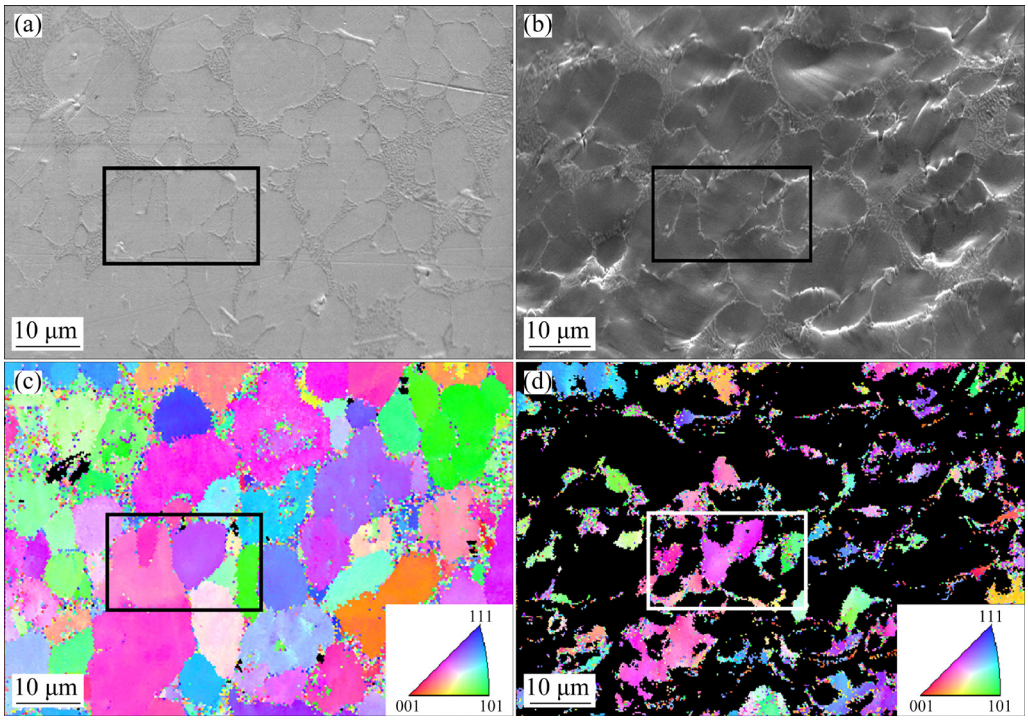

Fig. 5 Low magnification SEM images and corresponding IPFs of in-situ tension sample: (a, c) SEM image and IPF of sample in initial state, respectively; (b, d) SEM image and IPF of sample for same area in final state, respectively

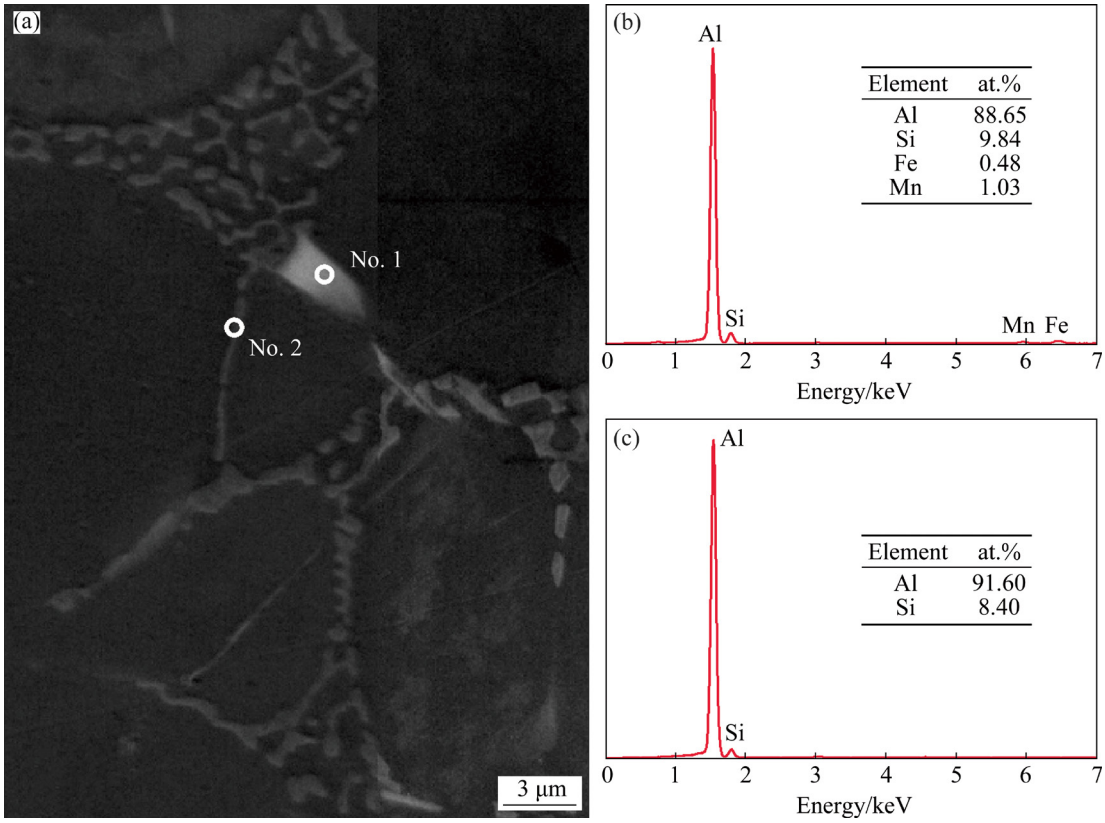

Fig. 6 Compositional analysis of second phases: (a) High magnification SEM image of area in Fig. 5(a); (b, c) EDS data for two typical second phase particles of No. 1 and No. 2 in (a), respectively

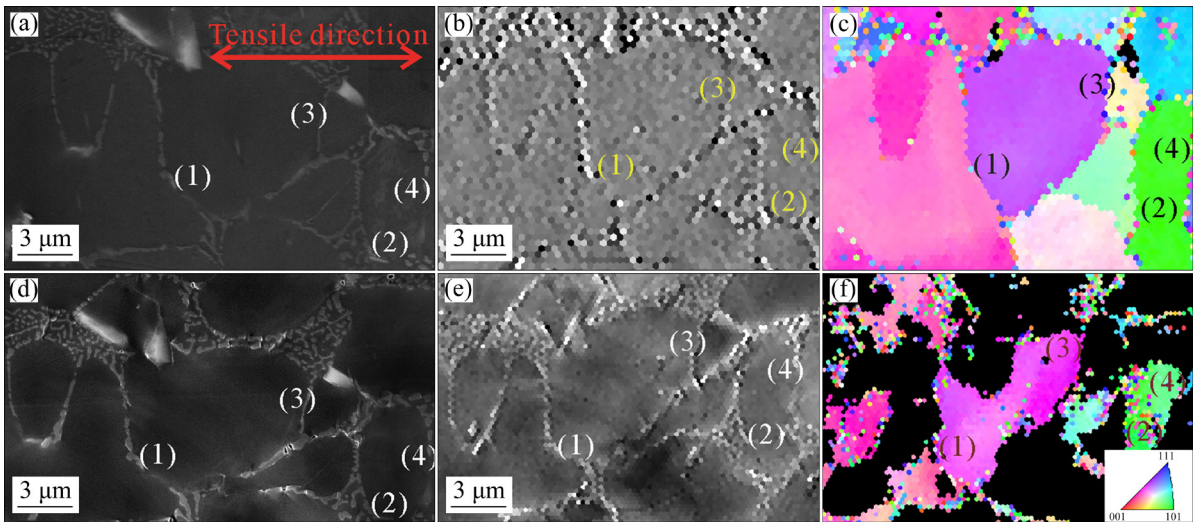

Fig. 7 SEM images (a, b, d, e) and IPFs (c, f) of same region in in-situ tension sample at initial (a−c) and final (d−f) states: (a, d) SE images collected before EBSD scan; (b, e) SE images collected during EBSD scan (denoted as SE-II)

The Si particles are mostly distributed at the grain boundaries (GB) in this alloy, and this phenomenon is common in Sr-modified Al−Si alloy [23].

It is reported that local GB deformation, which can be revealed by the orientation transformation of the regions nearby [24], affects the rotation of particles at the GB. Also, the EBSD study of CHEN et al [21] on an Al−Mg−Si alloy confirmed that there were multiple sub-grains formed in grains during deformation. Therefore, in the EBSD data analysis for the final state of the currently in-situ deformed sample, only the matrix near the particles

is focused on. The areas with strong enough signals are marked as (1), (2), (3) and (4) in Fig. 7(c).

The on-plane rotation of particles and neighboring grains in the four areas marked as (1), (2), (3) and (4) in Fig. 7 are summarized in Table 2. The negatives in ω_p mean counterclockwise on-plane rotation. The $|\Delta\omega|$ means the difference between grain rotation and particle rotation on the sample surface plane.

As shown in Table 2, the particles do rotate relatively to the neighboring grains more or less. In addition, ω_g also indicates the level of the local GB deformation, which displays little straightforward relationship with particle rotation. Besides, as the aim of this work is to confirm if the Si particles rotate with respect to the matrix grain or not, so in the following, the effect of Si particles' relative rotation would be discussed.

Table 2 Comparison between grain rotation (ω_g) and particle rotation (ω_p) on sample surface plane in four areas shown in Fig. 7

Area	ω_g	ω_p	$\lvert\Delta\omega\rvert$
(1)	7.88	−5.48	13.36
(2)	0.20	−9.30	9.50
(3)	2.44	4.59	2.15
(4)	0.20	−2.20	2.40

3.2 Effect of relative rotation of Si particles on mechanical properties

According to the dislocation theory of ASHBY [25] and NYE [26], the deformation at the interfaces of two-phase alloys is not uniform, and the gradient in the density of geometrically necessary dislocations (GNDs) is formed in the matrix near the particle. GNDs and statistically stored dislocations (SSDs) cause work-hardening effects. The elastic moduli of α(Al) phase (70 GPa) and the eutectic silicon phase (170 GPa) in Al−Si alloys are different [27], thus the local deformation will be uneven during relative rotation. Moreover, GNDs will also be generated near the GB in poly-crystalline alloys during tensile deformation [21,25]. According to the theory of ASHBY [25] and NYE [26], a hypothesis is proposed in this work: when a Si particle rotates relatively to the matrix grain where it is embedded, GNDs will be generated in the matrix to adapt to the deformation. Moreover, greater relative rotation can introduce a higher density of GNDs in the matrix nearby.

In this work, the variation of density of GNDs in matrix grains was qualitatively evaluated by KAM analysis of EBSD data [9,26,28,29] to reveal its correlation with the relative particle−matrix rotation, as shown in Fig. 8. The orange dashed

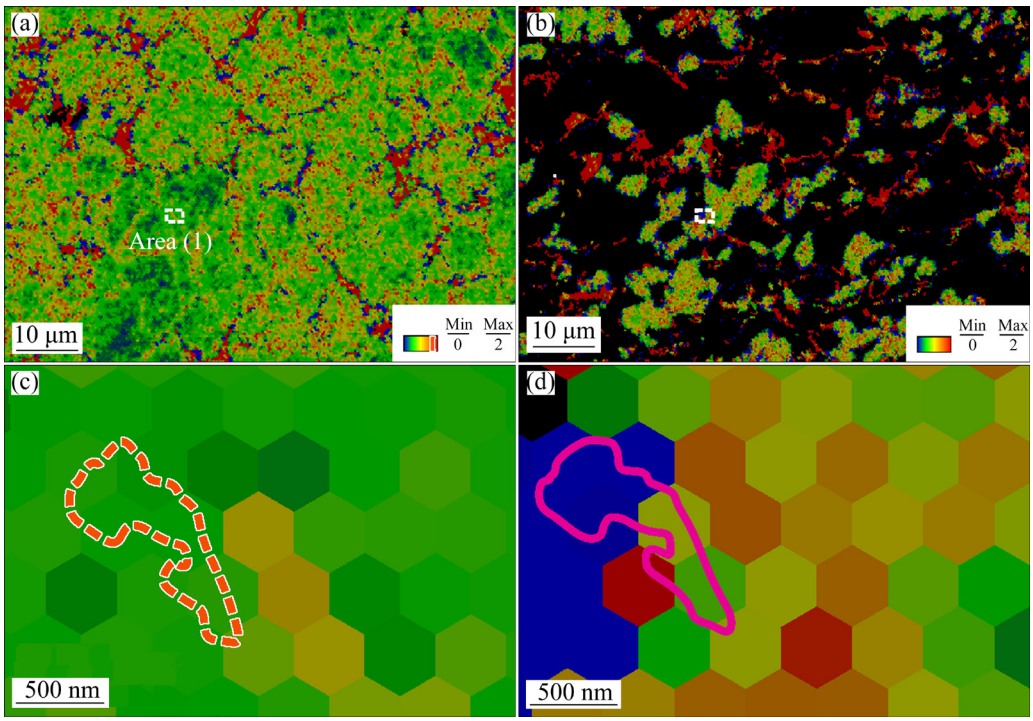

Fig. 8 KAM images: (a) Low magnification image in initial state; (b) Low magnification image in final state; (c) High magnification image of Area (1), i.e., white rectangle in (a); (d) High magnification image of white rectangle in (b)

curve in Fig. 8(c) is the outline of the particle in Area (1) in the initial state, and the purple solid curve in Fig. 8(d) corresponds to the final state. CALCAGNOTTO et al [13] proved that the distribution of KAM level obtained by EBSD data, which quantifies the average misorientation around a measurement point with respect to a defined set of neighboring points, was highly correlated to the density of GNDs.

The enlarged SEM image and corresponding KAM image are shown in Fig. 9, where the angles marked next to the symbol G represent the rotation angle of the grain on the sample surface plane. The blue axis r and angle θ are the rotation axis and rotation angle of the grain in the three-dimensional space. They were calculated by the "Symmetric Misorientations" operation in OIM analysis software. The superimposed dashed orange curves indicate the particle outlines in the initial state and the purple solid curves are for the final state. The numbers and arrows on the particles represent the angle and the direction of particle on-plane rotation, respectively. As mentioned above, the local deformation of GB (or the local grain rotation) can also generate GNDs nearby. According to the research of CHEN et al [21], the stronger the local deformation is, the higher the density of GNDs is. As shown in Fig. 9, the relationship between the relative rotation and the density of GNDs is obvious.

Phase boundaries and grain boundaries are both important. GNDs will be generated around these boundaries and relative rotation will occur in both cases. However, the main point of this research is whether the Si particles rotate with respect to the matrix grain and the main discussion is on the effects of the relative rotation, rather than grain boundary deformation. It should be stressed that the generation of GNDs near Si particles is mainly related to its rotation with respect to the matrix grain. Comparing Areas (1) and (2) with Areas (3) and (4) in Fig. 9, it can be found that a higher density of GNDs in the matrix will be generated when on-plane rotation angle between the particle and the embedding grain is larger and vice versa. The relationship is schematically shown in Fig. 10. It is also found that the rotation axis of grain is generally inclined with respect to the sample normal or sample parallels, such that a larger 3D rotation always corresponds to a larger on-plane rotation.

The relationship between particles and grains is significant for understanding the material deformation behavior. As shown in Fig. 10, when the relative rotation occurs, the deformation of the matrix near particles will not be uniform, the

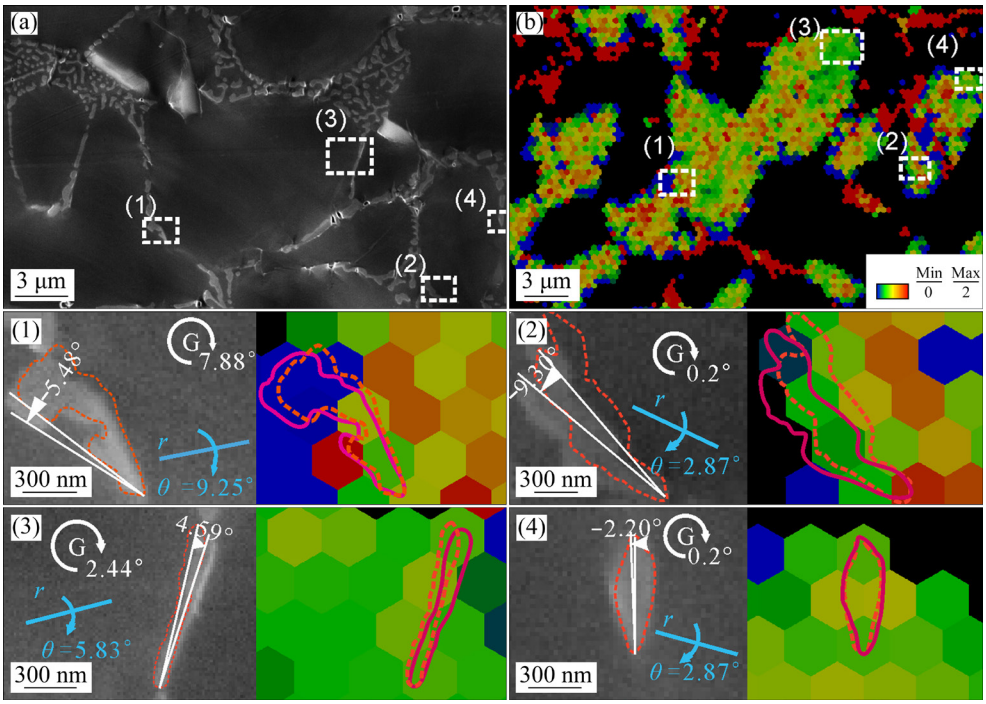

Fig. 9 Enlarged SEM (a) and corresponding KAM (b) images in finally deformed state (The enlarged SEM and KAM images of Areas ((1)−(4)) are shown at bottom; Area (1) is the same as that in Figs. 8(c) and (d))

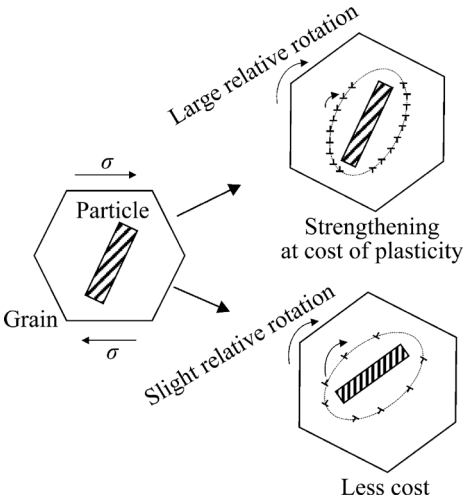

Fig. 10 Two kinds of relationship between particle and grain during deformation

dislocation loops and/or other forms of dislocations (called GNDs) will be generated around the particle [25]. Although the generation of GNDs due to geometrical constraints of the crystal lattice does not contribute to plastic strain, the GNDs act as obstacles to the motion of other dislocations [30]. Therefore, it can be concluded that the local work-hardening effect is increased by the generation of the GNDs, which has been proved to be correlated to the relative particle−matrix rotation in this work. Consequently, if a plastic metallic material needs to be strengthened (at the cost of the plasticity), embedding some fine dispersed rigid particles and causing their strong relative rotation during deformation will be helpful. In contrast, if plasticity is important for the same material, it is better to introduce some particles which only slightly rotate relatively to the matrix.

4 Conclusions

(1) The rotation of Si particles and α(Al) matrix grains in an Al−Si alloy was characterized by in-situ SEM observations and ex-situ EBSD, and compared on the same sample surface plane, to clarify whether the Si particles rotate with respect to the matrix grain. The KAM images, which reveal the variation in density of GNDs, were analyzed to discuss the effect of Si relative rotation on mechanical properties of the alloys.

(2) A new approach has been established such that the 3D grain rotation measured by EBSD can be projected onto the 2D sample surface plane, which can then be compared with the 2D on-plane particle rotation characterized by SEM.

(3) During tensile deformation of the Al−Si alloy, fine sub-micron Si particles were found to be rotated obviously with respect to α(Al) matrix grains.

(4) GNDs can be generated in the matrix near the Si particles due to the relative rotation between them. The stronger the relative rotation is, the higher the GND density is. A higher density of GNDs can cause larger work-hardening effect.

Acknowledgments

This work was financially supported by the National Natural Science Foundation of China (Nos. 52071340, 51820105001).

References

[1] YANG W Z, LIU Q C, YUE Z F, LI X D, XU B F. Rotation of hard particles in a soft matrix [J]. Journal of the Mechanics and Physics of Solids, 2017, 101: 285−310.

[2] YANG M J, CHEN H N, OREKHOV A, LU Q, LAN X Y, LI K, ZHANG S Y, SONG M, KONG Y, SCHRYVERS D. Quantified contribution of β'' and β' precipitates to the strengthening of an aged Al−Mg−Si alloy [J]. Materials Science and Engineering A, 2020, 774: 138776.

[3] DAVIS J R. Aluminum and aluminum alloys [M]. Ohio: ASM International, 1993.

[4] WANG Zhen-hong, ZHANG Li-tong, BIN SU, ZHANG Xiao-peng. Simulation on microstructure evolution of Al−Si alloy under effect of natural convection during solidification [J]. Transactions of Nonferrous Metals Society of China, 2022, 32(1): 79−90.

[5] PENG Hao-ping, LI Zhi-wei, ZHU Jia-qing, SU Xu-ping, YA LIU, WU Chang-jun and WANG Jian-hua. Microstructure and mechanical properties of Al−Si alloy modified with Al−3P [J]. Transactions of Nonferrous Metals Society of China, 2020, 30(3): 595−602.

[6] ZHANG N, TONG W. An experimental study on grain deformation and interactions in an Al−0.5%Mg multicrystal [J]. International Journal of Plasticity, 2004, 20 (3): 523−542.

[7] LI J J, CHEN S H, WENG G J, LIU C H. Stress-assisted grain-rotation-induced dislocation emission from grain boundaries in nanocrystalline face-centered-cubic metals [J]. Philosophical Magazine Letters, 2019, 99(12): 466−478.

[8] WANG L H, TENG J, LIU P, HIRATA A, MA E, ZHANG Z, CHEN M W, HAN X D. Grain rotation mediated by grain boundary dislocations in nanocrystalline platinum [J]. Nature Communications, 2014, 5(1): 1−7.

[9] NAGARAJAN S, JAIN R, GURAO N P. Microstructural characteristics governing the lattice rotation in Al−Mg alloy using in-situ EBSD [J]. Materials Characterization, 2021, 180: 111405.

[10] AGRAWAL H, GOKHALE A M, GRAHAM S, HORSTEMEYER M F, BAMMAN D J. Rotations of brittle

particles during plastic deformation of ductile alloys [J]. Materials Science and Engineering A, 2002, 328(1/2): 310−316.
[11] da FONSECA J Q, KO L. The kinematics of deformation and the development of substructure in the particle deformation zone [C]//The 36th Riso International Symposium on Materials Science. Roskilde: IOP Publishing, 2015: 012012.
[12] LI Y B, YANG M J, LI K, MA C D, YANG T, WANG J C, LU Q, ZHANG Y, LI G N, ZHANG S. In-situ study of effects of heat treatments and loading methods on fracture behaviors of a cast Al−Si alloy [J]. Materials Today Communications, 2021, 28: 102680.
[13] CALCAGNOTTO M, PONGE D, DEMIR E, RAABE D. Orientation gradients and geometrically necessary dislocations in ultrafine grained dual-phase steels studied by 2D and 3D EBSD [J]. Materials Science and Engineering A, 2010, 527(10): 2738−2746.
[14] BALASUNDARAM A, SHAN Z H, GOKHALE A M, GRAHAM S, HORSTEMEYER M F. Particle rotations during plastic deformation of 5086 aluminum alloy [J]. Materials Characterization, 2002, 48 (5): 363−369.
[15] AGRAWAL H, GOKHALE A M, GRAHAM S, HORSTEMEYER M F, BAMMAN D J. Rotations of brittle particles during plastic deformation of ductile alloys [J]. Materials Science and Engineering A, 2002, 328(1/2): 310−316.
[16] TIBBALLS J. Al−Si substitution in Al(Fe,Mn)Si phases [J]. Key Engineering Materials, 1990, 44/45: 233−246.
[17] MONDOLFO L F. Aluminum alloys: Structure and properties [M]. London: Elsevier, 2013.
[18] COOPER M. The crystal structure of the ternary alloy α (AlFeSi) [J]. Acta Crystallographica, 1967, 23(6): 1106−1107.
[19] KRAL M V. A crystallographic identification of intermetallic phases in Al−Si alloys [J]. Materials Letters, 2005, 59(18): 2271−2276.
[20] SUN Yu, PANG Shao-ping, LIU Xue-ran, YANG Zi-run, SUN Guo-xiong. Nucleation and growth of eutectic cell in hypoeutectic Al−Si alloy [J]. Transactions of Nonferrous Metals Society of China, 2011, 21(10): 2186−2191.
[21] CHEN P, MAO S C, LIU Y, WANG F, ZHANG Y F, ZHANG Z, HAN X D. In-situ EBSD study of the active slip systems and lattice rotation behavior of surface grains in aluminum alloy during tensile deformation [J]. Materials Science and Engineering A, 2013, 580: 114−124.
[22] BORKAR H, SEIFEDDINE S, JARFORS A E W. In-situ EBSD study of deformation behavior of Al−Si−Cu alloys during tensile testing [J]. Materials & Design, 2015, 84: 36−47.
[23] ZARIF M, MCKAY B, SCHUMACHER P. Study of heterogeneous nucleation of eutectic Si in high-purity Al−Si alloys with Sr addition [J]. Metallurgical and Materials Transactions A, 2011, 42(6): 1684−1691.
[24] ZAEFFERER S, KUO J C, ZHAO Z, WINNING M, RAABE D. On the influence of the grain boundary misorientation on the plastic deformation of aluminum bicrystals [J]. Acta Materialia, 2003, 51(16): 4719−4735.
[25] ASHBY M F. The deformation of plastically non-homogeneous materials [J]. The Philosophical Magazine: A Journal of Theoretical Experimental and Applied Physics, 1970, 21(170): 399−424.
[26] NYE J F. Some geometrical relations in dislocated crystals [J]. Acta Metallurgica, 1953, 1(2): 153−162.
[27] LIU X R, BEAUSIR B, ZHANG Y D, GAN W M, YUAN H, YU F X, ESLING C, ZHAO X, ZUO L. Heat-treatment induced defect formation in α-Al matrix in Sr-modified eutectic Al−Si alloy [J]. Journal of Alloys and Compounds, 2018, 730: 208−218.
[28] SUN S, ADAMS B L, KING W E. Observations of lattice curvature near the interface of a deformed aluminium bicrystal [J]. Philosophical Magazine A, 2000, 80(1): 9−25.
[29] SCHWARTZ A J, KUMAR M, ADAMS B L, FIELD D P. Electron backscatter diffraction in materials science [M]. New York: Springer, 2009.
[30] GAO H J, HUANG Y G. Geometrically necessary dislocation and size-dependent plasticity [J]. Scripta Materialia, 2003, 48(2): 113−118.

拉伸变形 Al−Si 合金中 Si 颗粒相对于晶粒旋转的原位证据

肖 遥[1]，兰新月[1]，鲁 强[1]，杜 勇[1,2,3]，李 凯[1,2,3]

1. 中南大学 粉末冶金国家重点实验室，长沙 410083；
2. 中南大学 轻质高强结构材料国防重点实验室，长沙 410083；
3. 中南大学 高等研究中心，长沙 410083

摘 要：为确定 Si 颗粒在拉伸变形过程中是否相对于基体晶粒发生旋转，采用原位拉伸扫描电子显微镜(SEM)和离位背散射电子衍射(EBSD)相结合的方法，研究 Al−Si 合金在拉伸变形过程中 Si 颗粒旋转与晶粒旋转之间的关系。通过对比晶粒的 EBSD 三维取向的平面投影信息与 Si 颗粒的原位 SEM 信息，发现 Si 颗粒在样品表面的平面上具有明显的相对旋转。此外，根据 EBSD 数据的中心点平均取向差(KAM)分析，发现 Si 颗粒的较大相对旋转会引入更高密度的几何必需位错(GND)，这会在颗粒附近的基体中产生较强的加工硬化效应。总之，Si 颗粒的相对旋转度越大，加工硬化效果越强。

关键词：Al−Si 合金；相对旋转；几何必需位错；原位拉伸；塑性变形；加工硬化效应

(Edited by Wei-ping CHEN)